# Generation of a Single-Cycle Optical Pulse

M. Y. Shverdin, D. R. Walker, D. D. Yavuz,* G. Y. Yin, and S. E. Harris

*Edward L. Ginzton Laboratory, Stanford University, Stanford, California 94305, USA*
(Received 20 July 2004; published 25 January 2005)

We make use of coherent control of four-wave mixing to the ultraviolet as a diagnostic and describe the generation of a periodic optical waveform where the spectrum is sufficiently broad that the envelope is approximately a single-cycle in length, and where the temporal shape of this envelope may be synthesized by varying the coefficients of a Fourier series. Specifically, using seven sidebands, we report the generation of a train of single-cycle optical pulses with a pulse width of 1.6 fs, a pulse separation of 11 fs, and a peak power of 1 MW.

It is now understood that the response of matter to optical radiation depends on the waveform of the instantaneous electric field as a function of time. In order to synthesize a periodic waveform that is not sinusoidal, it is required that the radiation be phase coherent across its spectrum and that the bandwidth of the radiation be large as compared to its central frequency. For each period of this waveform to be identical to every other period, it is also required that the ratio of the frequency of each sideband to the sideband spacing is an integer. If this ratio is noninteger, as is the case here, it is still possible to synthesize the *envelope* of the prescribed waveform. In effect the instantaneous electric field periodically sweeps through all values that are allowed by the synthesized envelope.

This Letter reports the generation of an optical pulse where the spectral bandwidth is larger than the central frequency. When the spectrum is phase locked, this produces a single-cycle pulse [1]; varying the phases produces other temporal shapes. The essential ingredient of this work, as compared to earlier work in our laboratory [2,3], is the use of nonresonant, four-wave frequency mixing in Xe as a diagnostic of the synthesized pulse envelopes. By using seven sidebands spaced by 2994 cm$^{-1}$, we describe the generation of a train of single-cycle optical pulses with a pulse width of 1.6 fs, a pulse separation of 11 fs, and a peak power of 1 MW. Since the central wavelength of our spectrum is 650 nm, this corresponds to a pulse less than 0.8 cycles long [4].

To obtain a multioctave phase coherent spectrum, we drive the fundamental vibrational transition in D$_2$ (Fig. 1). This produces a set of equidistant, mutually coherent sidebands that are separated from each other by the difference of the frequencies of the driving lasers and extend from 2.94 $\mu$m in the infrared to 195 nm in the ultraviolet [5]. A prism is used to disperse the sidebands, and a subset of seven sidebands extending from 1.56 $\mu$m to 410 nm is sent through a liquid crystal spatial light modulator where the phases of these sidebands are independently adjusted to Fourier synthesize the desired waveform in a target Xe cell. The phases are adjusted to compensate for the dispersion of

the intervening optics and for the Gouy phase shift of propagating spectral components [6,7].

With the incident Raman frequencies denoted by $\omega_q$, the frequency mixing process generates six ultraviolet frequencies at the frequency combinations $\omega_i + \omega_j - \omega_k$, with wavelengths from 365 to 236 nm (Fig. 1). By changing the relative phases of the incident Raman sidebands with the liquid crystal array, we change the temporal shape of the generated waveform and thereby control the relative amplitudes of the generated ultraviolet frequencies. Equivalently, but viewed in the frequency domain, we change the relative amplitudes of the interfering quantum paths at each of the generated frequencies. In this way we are able to maximize or minimize the total generated ultraviolet radiation or, instead, invert the ratio of selected UV sideband energies. By choosing the phases that maximize the four-wave mixing signal at all ultraviolet frequencies, we form the shortest pulse envelope that this spectrum (1.93 octaves in width) can make. As explained below, the shape of the temporal envelope is verified by
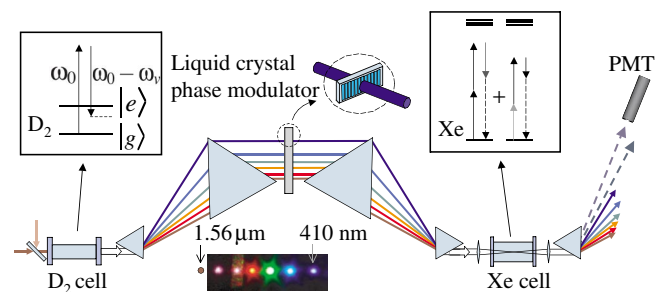


FIG. 1 (color). Experimental setup for temporal synthesis and characterization. Seven Raman sidebands are dispersed and their phases are independently varied by a liquid crystal modulator. The sidebands are recombined and focused into a target Xe cell. A solar-blind photomultiplier (PMT) measures UV radiation that is generated in the Xe cell. The intensity of the generated UV wavelengths depends on the relative phases and amplitudes of the incident optical signal. (The 1.56 $\mu$m sideband is not seen by the camera.)

electronically synthesizing and cross correlating two generated pulses in the target Xe cell.

We now cite related work: Using the same Raman generator, Sokolov *et al.* measured near-single-cycle-pulse structure [2]. Yavuz and colleagues produced a comb of about 200 spectral components and adjusted the phases of 15 of these sidebands, synthesizing a quasiperiodic waveform with pulse envelopes about three cycles long [3]. Using a related impulsive approach, Wittmann *et al.* produced a sequence of compressed femtosecond pulses [8]. Bartels *et al.* have shaped the pump pulse to optimize high-harmonic generation [9]. Losev and Lutsenko [10] suggested and demonstrated on-resonance two color pumping, and Yoshikawa and Imasaka [11] suggested the application of multicomponent Raman spectra to femtosecond time-scale pulses. Rotational Raman spectra extending from the infrared to the ultraviolet have been demonstrated [12]. Liang and colleagues used solid hydrogen for collinear Raman sideband generation [13]. The synthesis of ultra-broadband solitons has been suggested by Kaplan [14] and by Yavuz *et al.* [15]. Short time-scale work that is based on the Raman technique comprises a small subset of a broad effort on femtosecond and attosecond pulse synthesis; we will not attempt to summarize this work.

The principal components that are used to generate a temporal waveform of a desired shape are the Raman generator, the optics for dispersing and recombining the beam, and the 640 pixel liquid crystal phase modulator (Fig. 1). The Raman frequency components are focused to the center of a Xe target cell where a four-wave frequency mixing is used to generate the six ultraviolet beams. We use a four-wave frequency process of the type $\omega_u = \omega_i + \omega_j - \omega_k$ rather than third harmonic generation because the former process allows focusing to the center of a target cell, while the latter process does not [16]. As in Ref. [2], we drive the fundamental vibrational transition of deuterium ($D_2$) by two transform-limited laser pulses, one from a Nd-doped yttrium aluminum garnet laser at 1.064 $\mu$m and the other from a Ti:Sapphire laser at 807 nm, such that their frequency difference is approximately equal to the transition frequency of 2994 cm$^{-1}$. The energy and pulse width of the 1.064 $\mu$m beam are 70 mJ and 10 ns. For the 807 nm beam these quantities are 60 mJ and 15 ns. Both have a repetition rate of 10 Hz and are combined and loosely focused into a 50 cm long $D_2$ cell. At the focus, the spot sizes of the 1.064 $\mu$m and 807 nm beams are 1.1 mm and 600 $\mu$m, with corresponding intensities of $\approx$ 1 GW/cm$^2$. The Raman transition is driven 700 MHz below resonance, allowing us to adiabatically prepare a large molecular coherence. To increase the ground state population and to reduce Doppler and collisional linewidths, the cell is cooled by liquid nitrogen.

The generated Raman beam is expanded and collimated by a pair of fused silica lenses. To avoid damage to the liquid crystal spatial light modulator, the beams are passed through two interference filters that selectively attenuate the strong 1.064 $\mu$m and 807 nm beams. The spectrum is dispersed with a pair of fused silica prisms, and all sidebands with a wavelength shorter than 410 nm are blocked. The distances and the angles between the prisms are chosen so that the dispersed beams are parallel and spatially resolved as they pass through the liquid crystal. The liquid crystal modulator consists of a linear array of 640 pixels, each 97 $\mu$m wide and spaced by 3 $\mu$m. The refractive index of each sideband is controlled by applying a calibrated voltage. We are constrained to seven sidebands by the bandwidth of the liquid crystal. Because the liquid crystal acts as a weak etalon, the transmitted energy of each Raman sideband varies by up to 10% as the voltage applied to the liquid crystal is changed. This variation is measured and included in the calculations. After phase adjustment, the sidebands are spatially recombined with another prism pair and focused into an 8 cm Xe cell at a pressure of 100 torr with an $f = 20$ cm achromatic lens. The total intensity at the focus is $\approx 40$ GW/cm$^2$. A four-wave mixing signal is generated with an efficiency which varies, depending on the spectral component, from $10^{-12}$ to $10^{-8}$ and is measured by a solar-blind photomultiplier. The photomultiplier is calibrated using our Raman source. The uncertainty of this calibration is 25%.

Figure 2 shows the relative intensities of six of the generated ultraviolet wavelengths for four sets of incident phases or, equivalently, for four different temporal waveforms. In each part of this figure, the energies of the incident Raman sidebands are the same (see figure caption). In Fig. 2(a), the relative phases are adjusted to maximize the total generated ultraviolet power. As will be verified below, these phases correspond to a single-cycle temporal waveform. In Fig. 2(b), the relative phases are adjusted to minimize the total generated ultraviolet power. These phases correspond to an incident frequency modulated (FM)-like temporal waveform. In Figs. 2(c) and 2(d), we set the phases to produce temporal waveforms that invert the ratio of the energies of 365 and 300 nm UV sidebands. We are able to adjust the sideband phases independently to within $0.1\pi$. The phase stability is good and shows no appreciable drift over several hours. Taking the phases in Fig. 2(a) to be zero, the phases of the 1.56 $\mu$m, 1.064 $\mu$m, 807 nm, 650 nm, 544 nm, 468 nm, and 410 nm sidebands of the FM-like spectrum of Fig. 2(b) are 0, 0, $\pi$, $\pi$, $\pi$, 0, and $\pi$ radians. The time domain waveform which corresponds to these phases exhibits a periodic chirp. The distribution of UV energies in Figs. 2(c) and 2(d) is more sensitive to small phase variations of the Raman sidebands and must be determined during each run by trial and error.

We next describe the technique for generating and cross correlating a train of single-cycle optical pulses. First, we set the phases to maximize the UV generation at each of the UV wavelengths [as in Fig. 2(a)]. This is done by adjusting
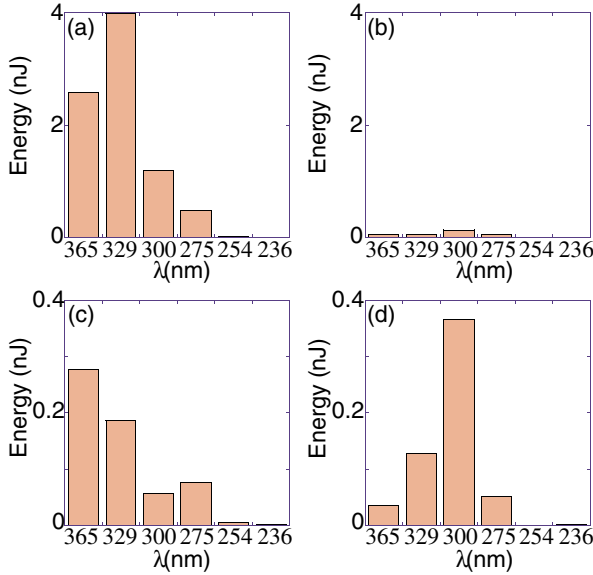
FIG. 2 (color online). Coherent control of the generated UV radiation. We plot the energies of the generated UV sidebands for different incident optical waveforms. Relative phases are adjusted to (a) maximize total UV generation, (b) minimize total UV generation, and (c),(d) invert the ratio of the energies at 365 and 300 nm. The energies of the incident Raman sidebands are approximately: 1.7 mJ at 1.56 $\mu$m; 2.5 mJ at 1.064 $\mu$m; 1.2 mJ at 807 nm; 2.5 mJ at 650 nm; 1.9 mJ at 544 nm; 0.8 mJ at 468 nm; and 0.5 mJ at 410 nm. [The energy at 254 nm in (d) was inadvertently not measured.]

the phase of individual Raman sidebands to maximize four-wave mixing efficiency, optimizing each sideband's phase in sequence until further adjustment no longer increases the UV generation. Numerical simulation of this phase optimization procedure shows that it consistently converges to the correct set of relative phases. As described below, the close agreement between the predicted and experimental cross correlations further verifies that the phases have been optimized. We then cross correlate these pulses as follows: We view the generated even-numbered sidebands as forming one optical pulse, and the odd sidebands as forming a second pulse, and electronically delay one pulse with respect to the other. The variable delay is attained by adding to each of the even sidebands a phase that is proportional to its frequency, while leaving the phases of the odd sidebands unchanged [3].

By varying this delay, and measuring the generated UV signal at 365 nm, we obtain the cross correlation of Fig. 3(a). By measuring the signal at 329 nm, we obtain the cross correlation of Fig. 3(b). The frequency of the Raman sidebands is $\omega_q = \omega_0 + q\omega_v$, where $\omega_0$ is the 807 nm pump laser frequency and $\omega_v$ is the vibrational modulation frequency. Figure 3(c) shows a third cross correlation which is obtained by delaying a pulse consisting of the three highest frequencies ($q = 2, 3, 4$) with respect to the four lowest frequency components ($q =$
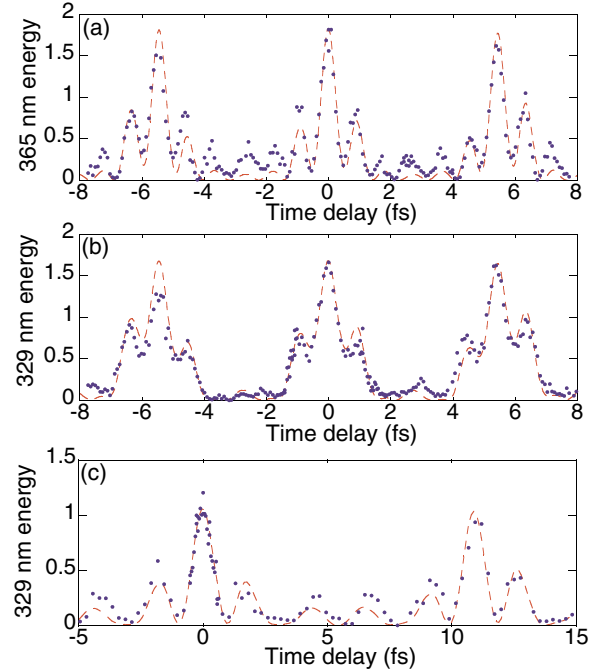


FIG. 3 (color online). Correlation of single-cycle waveforms. We electronically synthesize two pulses consisting of two subsets of the Raman spectra and delay one pulse with respect to the other. We measure the four-wave mixing signal (points) at 329 nm as a function of the relative delay and plot the corresponding theoretical trace (dashed lines) normalized at the peak. In (a) and (b), the pulse consisting of sidebands $q = -2, 0, 2, 4$ is delayed with respect to the $q = -1, 1, 3$ pulse. In (c), the pulse consisting of the $q = 2, 3, 4$ sidebands is delayed with respect to the $q = -2, -1, 0, 1$ pulse. Each experimental point is an average of 50 laser shots. Energies are in arbitrary units.

$-2, -1, 0, 1$). The peak-to-trough contrast of $\approx 100:1$ indicates well-formed pulses rather than structure imposed on a noisy background.

The dashed lines in all parts of Fig. 3 show the results of a theoretical calculation of the expected temporal cross correlations. Experiment and theory are matched at their peaks at each of the generated UV wavelengths. The agreement for all time delays is good. The width and the period of each cross-correlation profile scale inversely with the bandwidth and the frequency separation, respectively, of the correlated subsets of sidebands. Consequently, the correlation traces in Fig. 3(c) have approximately twice the width and period as those in Figs. 3(a) and 3(b). The large central peak with sidelobes of much smaller amplitude is the signature of a single-cycle pulse.

Our model of the four-wave frequency conversion process is based on a formalism for optical frequency conversion with Gaussian beams that have different confocal parameters [17]. The contribution of the sidebands to the dipole moment at each generated ultraviolet frequency is of the form $P(\omega_u) \propto \sum A_{ijk} E_i E_j E_k^*$. The weighting factors $A_{ijk}$ of the different paths include the detunings from
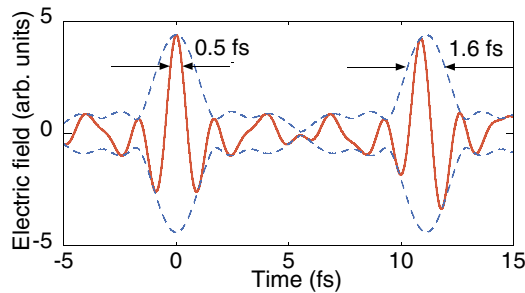
FIG. 4 (color online).    The theoretically predicted electric field (thick line) and the corresponding field envelope (dashed line) that are synthesized by setting all of the Raman sideband phases to zero. The FWHM of the pulse envelope is 1.6 fs. The cosine pulse (left) is 0.5 fs long.

resonance and the effects of the differing confocal parameters on phase matching. The nonlinear susceptibility is calculated by modeling the Xe atom as a ground state and two opposite parity states at $75\,000$ cm$^{-1}$ [18].

Of importance, the correlation traces exhibit the expected carrier-envelope phase slip. Maximizing the generation of each UV sideband matches the peak of the electric field with the peak of the intensity envelope for one of the pulses in the pulse train. But because the frequencies of the 1.064 $\mu$m and 807 nm driving lasers are not integer multiples of their frequency difference, the other pulses in the pulse train have a nonzero carrier-envelope offset [19]. At zero pulse delay, we predict and observe a symmetric cross-correlation trace. The sidelobes of the pulses that are centered at other delays are asymmetric and their shape is in agreement with theory.

Figure 4 shows the calculated single-cycle waveform which generates the predicted cross-correlation profiles of Fig. 3. This plot is obtained by using the measured intensities of the respective Fourier components and assuming (based on the previous correlation profiles and their agreement with theory) that the phases are equal. The FWHM of the intensity envelope is 1.6 fs and the pulse width is 0.5 fs for waveforms with zero carrier-envelope offset. The sidelobes have an intensity of 30% of the peak. This may be compared to the theoretical value of 23% if the amplitudes of the spectral components were equal.

Because the ratio of the sideband frequency to the sideband spacing is noninteger, this work has demonstrated the synthesis of a train of single-cycle pulses which vary under the synthesized envelope. In the future, it should not be overly difficult to make a source where the ratio of the sideband frequency to the sideband spacing is an integer. As an example, if the Raman vibrational frequency is $\omega_v$, then one might use an optical parametric oscillator pumped at a frequency of $3\omega_v$ to generate a signal at $2\omega_v$ and an idler at $\omega_v$. These latter frequencies would pump the Raman cell. For $H_2$, the vibrational frequency

is 4155 cm$^{-1}$ and the necessary pumping wavelength is 802.2 nm.

In summary, we have synthesized and characterized a train of high peak power, single-cycle pulses. We have also shown the ability to synthesize other pulse envelopes, for example, an FM-like envelope. An essential ingredient in this experiment is the use of four-wave mixing to the UV as a diagnostic of the synthesized envelopes.

*Present address: Physics Department, University of Wisconsin at Madison, Madison, WI 53706, USA.
[1] D. You and P. H. Bucksbaum, J. Opt. Soc. Am. B **14**, 1651 (1997).
[2] A. V. Sokolov, D. R. Walker, D. D. Yavuz, G. Y. Yin, and S. E. Harris, Phys. Rev. Lett. **87**, 033402 (2001).
[3] D. D. Yavuz, D. R. Walker, M. Y. Shverdin, G. Y. Yin, and S. E. Harris, Phys. Rev. Lett. **91**, 233602 (2003).
[4] Thomas Brabec and Ferenc Krausz, Phys. Rev. Lett. **78**, 3282 (1997).
[5] A. V. Sokolov, D. R. Walker, D. D. Yavuz, G. Y. Yin, and S. E. Harris, Phys. Rev. Lett. **85**, 562 (2000).
[6] S. E. Harris, J. J. Macklin, and T. W. Hänsch, Opt. Commun. **100**, 487 (1993).
[7] F. Lindner, G. G. Paulus, H. Walther, A. Baltuska, E. Goulielmakis, M. Lezius, and F. Krausz, Phys. Rev. Lett. **92**, 113001 (2004).
[8] M. Wittmann, A. Nazarkin, and G. Korn, Phys. Rev. Lett. **84**, 5508 (2000).
[9] R. Bartels, S. Backus, E. Zeek, L. Misoguti, G. Vdovin, I. P. Christov, M. M. Murnane, and H. C. Kapteyn, Nature (London) **406**, 164 (2000).
[10] L. L. Losev and A. P. Lutsenko, Quantum Electron. **23**, 919 (1993).
[11] S. Yoshikawa and T. Imasaka, Opt. Commun. **96**, 94 (1993).
[12] H. Kawano, Y. Hirakawa, and T. Imasaka, Appl. Phys. B **65**, 1 (1996).
[13] J. Q. Liang, M. Katsuragawa, F. LeKien, and K. Hakuta, Phys. Rev. Lett. **85**, 2474 (2000).
[14] A. E. Kaplan, Phys. Rev. Lett. **73**, 1243 (1994).
[15] D. D. Yavuz, A. V. Sokolov, and S. E. Harris, Phys. Rev. Lett. **84**, 75 (2000).
[16] G. C. Bjorklund, IEEE J. Quantum Electron. **11**, 287 (1975).
[17] G. Hilber, D. J. Brink, A. Lago, and R. Wallenstein, Phys. Rev. A **38**, 6231 (1988).
[18] The full calculation is described in M. Y. Shverdin, Ph.D. thesis, Stanford University, 2004.
[19] T. Udem, R. Holzwarth, and T. W. Hänsch, Nature (London) **416**, 233 (2002).